PWM-Scaled Hard- and Soft-Iron Compensation for Motor-Induced Magnetometer Distortion

2808780 2073403 2627512 2791828

***Abstract*—This project investigates how motor-induced magnetic interference affects the readings produced by the LIS3MDL magnetometer on the Pololu 3Pi+ robot. The challenge arises from hard-iron and soft-iron distortions generated by the robot's motors, batteries, and surrounding conductive components, all of which alter the measured magnetic field. The study focuses on quantifying these distortions over a range of motor PWM values and assessing whether a compensation model can be constructed to mitigate their effect using a deformation matrix scaled proportionally to the supplied PWM. The results show that this is mathematically feasible and evidence of its success are included. Difficulties were found in determining the relationship between soft-iron distortion and PWM value due to the limited trials and small range of PWM values tested. However, hard-iron distortion was successfully mitigated throughout the range, and soft-iron distortion was significantly reduced in a proof-of-concept implementation of this method.**

I. Introduction

The Polulu 3Pi+ 32U4 is equipped with the LIS3MDL 3-axis digital output magnetometer [1]. This magnetometer employs Anisotropic Magneto-Resistance (AMR), a principle in electromagnetism that states that the electrical resistance of certain materials changes based on the orientation of the magnetic field relative to the material's magnetisation direction [2].

The chip contains three independent AMR sensing elements, each oriented to measure the magnetic field along the device's x, y, and z axes. When the chip is exposed to an external magnetic field, the resistance of each sensing element changes. Stronger fields and specific field angles create larger changes in electrical resistance. These changes are processed by the Analog-to-Digital Converter (ADC), which converts the analog voltage changes, caused by the resistance changes from each sensor, into a digital value for the microcontroller. Factory calibration values are applied to give meaning to the readings relative to a zero-Gauss level [3], which corresponds to readings obtained when not exposed to any magnetic field.

Section 4.3 of the magnetometer documentation [1] warns of errors in compass heading caused by high-current wiring, due to conductor-generated magnetic fields combining with the Earth's magnetic field. These errors are classified as hard-iron and soft-iron distortions some of which are from the 3pi+ itself. These include magnets in the motors and encoders, electrical currents through the board, and hard iron distortions from metal. Hard-iron distortion is depicted in two dimensions as a translation of the average magnitude of readings [4], obtained by rotating the magnetometer about the gravity axis. Hard-iron effects are caused by permanent magnets or magnetized ferromagnetic components fixed relative to the sensor. Soft-iron distortion is depicted in two dimensions as an elliptical deformation of the ideal, circular result, where the eccentricity of the resulting ellipse is proportional to the degree of soft-iron distortion present [4]. Soft-iron effects are introduced by ferromagnetic materials that distort the local magnetic field by altering the magnetic flux lines [5] The inherent soft-iron and hard-iron effects were determined by rotating the robot by hand while intermittent magnetometer readings were collected. The results were visualised in two dimensions, Fig. 1. A significant offset was observed from the ideal case of results centred at zero magnitude. The shape was largely circular; however, it was clear that the eccentricity was nonzero.

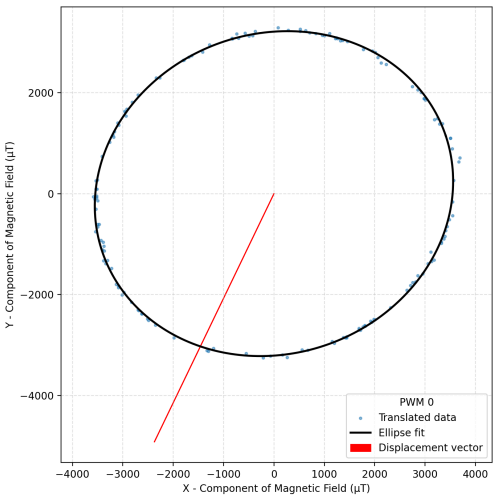

Fig. 1: *Raw magnetometer readings for 0 PWM, re-centred to the origin with ellipse fitted via least-square method. Red line shows the vector from the center of the raw, uncompensated, data to the origin. The black ellipse is used to estimate the eccentricity of the data.*

Applying an elliptical least-squares fit to the data, Fig. 1, revealed an estimated eccentricity of 0.471 and a displacement from the origin with magnitude approximately 5462. Conducting the same analysis on data collected while the robot's motors were active with 100 PWM, yielded an estimated eccentricity of 0.510 and a displacement vector of approximately 5188.

These observations agree with the mathematical model [6] where the measurement vector $\tilde{\mathbf{m}}$ consists of a combination of Earth's magnetic field and magnetic fields created by nearby disturbances:

$$\tilde{\mathbf{m}} = \mathbf{S_I^{-1}}(\mathbf{m_E} + \mathbf{m_e}(t)) + \mathbf{b_{HI}} + \mathbf{m_i}(t)$$

where $\mathbf{m_e}(t)$ is the environmental noise, $\mathbf{m_i}(t)$ is the internal noise, $\mathbf{m_E}$ is the Earth's magnetic field vector, $\mathbf{S_I^{-1}}$ is the inverse soft-iron distortion matrix, and $\mathbf{b_{HI}}$ is the hard-iron displacement vector. In this paper, we treat hard-iron distortion as the sum $\mathbf{b_{HI}} + \mathbf{m_i}(t)$ due to the difficulty of separating internal sensor noise from robot-internal magnetic disturbances. Combining the initial

observations with this model suggests that the motors cause soft-iron distortion but have little hard-iron impact caused by the metallic gears. Therefore, a compensation matrix for soft-iron distortion will need to be scaled proportionally to supplied PWM to motors, while hard-iron compensation is expected to be a constant translation of results.

A static compensation model can be constructed to account for the hard-iron and soft-iron distortions present in the local magnetic field. Ignoring the time-varying environmental and internal noises $\mathbf{m_e}(t)$ and $\mathbf{m_i}(t)$, rearranging the equation above yields an estimate for the Earth's magnetic field:

$$\mathbf{m_c} = \mathbf{S_I}\left(\tilde{\mathbf{m}} - \mathbf{b_{HI}}\right)$$

where $\mathbf{m_c}$ is the compensated magnetometer reading, which should equal $\mathbf{m_E}$ when no time-varying noise or external field is applied [6].

This paper aims to explore, quantify, and mitigate both the soft-iron and hard-iron effects induced by active motor operations over a range of supplied PWM values. Discussed in detail in section III, the methodology ensures maximum control over any variable that is expected to affect the magnetometer readings, resulting in a repeatable experiment with uncertainty estimates for each metric used.

A. Hypothesis Statement

> *Implementation of the theoretical compensation model to mitigate soft- and hard-iron distortion from magnetometer readings prompts an investigation into the scaling of the distortions relative to supplied PWM values. We hypothesise that a compensation model can be created for the 3Pi+ robot that scales proportionally to the PWM supplied to the motors to mitigate the soft- and hard-iron distortion both inherent to the robot, and induced by the motors.*

Section II describes the investigation design, stating the physical set-up and software used throughout the experiment. Section III contains a discussion of the method used, and a discussion of variables and metrics. Section IV presents the findings from the experiment and section V assesses the effectiveness of the obtained solution.

II. Implementation

A. Experiment Workstation

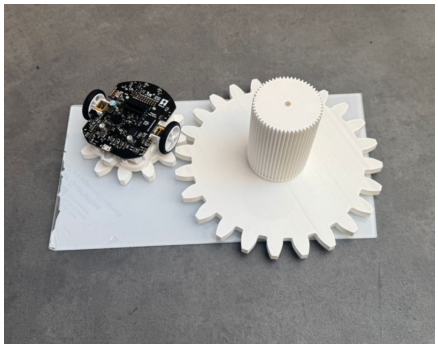

Fig. 2: An image of the workstation with the robot

To ensure the reproducibility of the experiments and isolate the magnetometer readings as the dependent variable, a custom workstation was developed. As shown in Fig. 2, it consists of a dual-gear mechanism, with a manually operated driver gear and a driven gear equipped with a mount to secure the robot. All components of the workstation were fabricated from acrylic and 3D-printed PLA to prevent the introduction of external magnetic interference.

The base of the workstation was secured to the ground using adhesive tape, and the gears were supported within the acrylic frame with 3D-printed holders to constrain the robot's movement to a fixed rotary axis. The robot mount was designed to elevate the chassis to allow the wheels to spin freely. This configuration ensured a single degree of freedom, eliminating slippage and axial tilt that would otherwise occur in free-roaming ground tests. By mechanically restricting the axis of rotation, it ensured consistent position within the Earth's magnetic field, certifying that only changes in the supplied PWM were responsible for any changes observed in the data collected.

Additionally, the workstation was situated away from metallic materials and power sockets, and the operator conducting the experiment was required to remove all metallic objects. This ensured that the operator's proximity and the surrounding did not introduce external distortions.

B. Data Collection

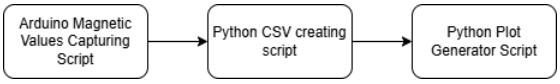

Fig. 3: Script pipeline flow

Algorithm 1 Spin Robot & Capture Unique Magnetometer Samples

Input: Magnetometer sensor, motors
Output: Array of unique readings L

$MaxLogs \leftarrow 150$
$LogInterval \leftarrow 10$ ▷ ms
Motors.setPWM($Speed, Speed$)
$LastReadTime \leftarrow$ current time
$(LastX, LastY, LastZ) \leftarrow$ sentinel values
$LogIndex \leftarrow 0$

while $LogIndex < MaxLogs$ **do** ▷ Capture Loop
  $Now \leftarrow$ current time
  if $Now - LastReadTime \geq LogInterval$ **then**
    $LastReadTime \leftarrow Now$
    Read magnetometer (x, y, z)
    if (x, y, z) differs from $(LastX, LastY, LastZ)$ **then**
      $L[LogIndex] \leftarrow (x, y, z)$
      $LogIndex \leftarrow LogIndex + 1$
      $(LastX, LastY, LastZ) \leftarrow (x, y, z)$
    end if
  end if
end while
Motors.stop()

while true **do** ▷ Report Data on Request
  if Serial receives 'r' **then**
    for $i \leftarrow 0$ to $LogIndex - 1$ **do**
      Serial.print($L[i]$)
    end for
  end if
end while

Minimising external electromagnetic interference was crucial to the experiment. This forced data collection to be done offline, and data to be uploaded after collection was complete. Due to the significant memory limitations of the 3Pi+ robot, a maximum of 150 values could be stored from each axis. To maximise the importance of each datapoint stored, updated values were checked against the previous values to prevent duplicates. Early tests revealed that update calls to the magnetometer did not always result in updated values. This behaviour, combined with the impossibility of maintaining exact rotation speeds across experiments, forced the use of a stochastic sampling method. This also allowed uncertainty estimates to be obtained using the standard error of the calculated metric over multiple trials. During a trial, the robot periodically attempted to update the magnetometer readings, and new values were stored in memory. Identical software was used for all trials, except for the change in PWM supplied to the motors throughout the collection process. When data collection was complete, the robot was reconnected to Serial, and the data could be output for analysis.

III. Experiment Methodology

The Pololu 3Pi+ robot was tasked with reading the magnetic field strength while its motors were active in forward rotation. Specifically, the experiment evaluates the possibility of a dynamic compensation model by measuring how hard- and soft-iron distortions become greater as the power supplied to the motor increases.

A. Overview of Method

The experiment followed a circular sweep procedure to generate a dataset of magnetic field readings. The robot was secured in the workstation described in Section II. This setup allowed the wheels to spin at different speeds while the chassis remained constrained to a fixed axis rotation. Suspending the wheels ensured that the magnetic influence did not come from surface-induced vibration or wheel slip.

- Step 1: The workstation was manually actuated via the driver gear to establish a steady rotational velocity.
- Step 2: With the robot in motion, the motors were initialised to run at a target PWM on both wheels.
- Step 3: The robot immediately began sampling raw magnetometer readings in x, y, and z at fixed intervals.
- Step 4: Once 150 magnetometer readings were collected, the motors were halted, and the data was offloaded via the serial interface.
- Step 5: Batteries were tested and recharged if the recorded voltage had dropped by more than $0.5V$ from the fully charged state.

This process was repeated 3 times at each PWM interval. While the number of trials was limited, the resulting dataset contained a large number of points that ensured a high-density point graph, allowing robust analysis.

B. Mathematical Methods

Hard-Iron Distortion:
Computation of a translation vector that compensates for hard-iron distortion, was done by fitting an ellipse to the two-dimensional magnetometer data. The translation vector is then taken as the algebraic centre of the ellipse,

$$\boldsymbol{b}_{HI} = (x_c, y_c)^\top.$$

This vector was subtracted from each data point to correct for the hard-iron distortion, producing centred data about the origin.

Soft-Iron Distortion:
Computation of a deformation matrix that compensates for soft-iron distortion, was started by fitting an ellipse to the two-dimensional magnetometer data. Any ellipse centred at the origin can be written as

$$\boldsymbol{x}^\top A \boldsymbol{x} = c,$$

where $\boldsymbol{x} = \big(x,\ y\big)$, A is a symmetric positive-definite matrix, and $c > 0$ is a constant determined by the ellipse. Since A is symmetric, it admits the eigendecomposition

$$A = PDP^\top,$$

where P is an orthogonal matrix whose columns are the eigenvectors of A, and

$$D = \mathrm{diag}(\lambda_1, \lambda_2)$$

contains the corresponding positive eigenvalues. These eigenvalues determine the ellipse's semi-axes:

$$a = \frac{1}{\sqrt{\lambda_1}}, \qquad b = \frac{1}{\sqrt{\lambda_2}}.$$

The matrix $P^\top$ rotates the ellipse into alignment with the coordinate axes, and D contains the stretching and squashing along those axes.
We seek a linear map S_I such that $\boldsymbol{y} = S_I \boldsymbol{x}$ converts

$$\boldsymbol{x}^\top A \boldsymbol{x} = c \quad \text{into} \quad \boldsymbol{y}^\top \boldsymbol{y} = c,$$

a circle with radius $\sqrt{c}$.
Substituting in the decomposition, $A = PDP^\top$, gives:

$$\boldsymbol{x}^\top PDP^\top \boldsymbol{x} = c.$$

Transformed coordinates, defined as

$$\boldsymbol{y} = D^{1/2} P^\top \boldsymbol{x},$$

then form the equation of the circle,

$$\boldsymbol{y}^\top \boldsymbol{y} = \boldsymbol{x}^\top PDP^\top \boldsymbol{x} = c,$$

with radius $\sqrt{c}$.
Therefore, the soft-iron compensation matrix is

$$S_I = D^{1/2} P^\top.$$

Applying a scale factor to this matrix should allow the soft-iron distortion to be compensated for the full PWM range. However, this is only possible if the orientation of the ellipse is unchanged through varying PWM. This is because applying a scale factor to the compensation matrix is equivalent to applying the scale factor to $D^{1/2}$ which contains only the stretching and scaling information of the compensation. If the orientation varies across the PWM range, then the scaling will not be applied in the correct directions, which cannot be resolved by scaling the matrix as this information is encoded in the eigenvectors. Therefore, soft-iron compensation can be scaled over a PWM range if the orientation of semi-major and semi-minor axes are independent of the power supplied to the motors.

C. Discussion of Variables

1) Independent Variable: In this study, the independent variable is the **Pulse Width Modulation (PWM) duty cycle** supplied to the motors. This value directly modulates the current draw (ΔI) and rotational speed of the DC motors, thereby altering the strength of the conductor-generated magnetic fields that interfere with the LIS3MDL sensor [7].

Three distinct $\text{PWM}_{\text{motor}}$ values were selected to characterize the effect of motor activity across the operational range: Three distinct $\text{PWM}_{\text{motor}}$ values were selected to characterize the effect of motor activity across the operational range:

$$\text{PWM}_{\text{motor}} \in \{0, 50, 100, 150\}$$

The observed effect is attributed to the change in current (ΔI) within the motor windings, which modulates the resultant magnetic flux ($\Delta\Phi$) experienced by the sensor.

2) Extraneous Variables: These variables are unknowns that may affect the dependent variable. Details of efforts made to mitigate their affects are included here.

- **Data Collection Duration:** The time spent collecting raw data was dependent on the rate of successful updates to magnetometer readings. Data collection continued until 150 unique results were stored.
- **Data Collection Frequency:** The period between magnetometer updates was unknown due to early tests revealing inconsistent magnetometer updates. To optimise the storage on the robot, data was only stored if it differed from the previous reading. This stochastic sampling forced multiple trials to ensure reliable data, however, mitigated the affects of inconsistent rotation speed of the robot.
- **Rotation Speed:** The robot was rotated manually for all trials. While care was taken to keep the rotation as constant as possible, variation was unavoidable. Due to the stochastic sampling method, a variety of speed benefits the statistical reliability of the results over enough trials.

3) Dependent Variables: The core dependent variable collected during the experiment was:

- **Magnetometer Readings ($\mathbf{m}$):** The raw digital values recorded from the three orthogonal axes of the LIS3MDL sensor on Pololu 3p+, represented as $\mathbf{m} = (m_x, m_y, m_z)$. These readings are analyzed to observe the effects of motor operation, specifically distinguishing between **hard-iron distortion** ($\mathbf{b}_{HI}$) and **soft-iron distortion** ($\mathbf{S}_I^{-1}$).

4) Controlled Variables:

- **Environmental Magnetic Interference ($\mathbf{m}_e$):** The experiment was conducted at a fixed location, isolating the set-up from external nearby ferrous materials. The custom workstation employed non-ferromagnetic materials (PLA and acrylic) to prevent the introduction of magnetic interference external to the robot.
- **Data Acquisition System:** The robot operated autonomously (offline) without a physical USB connection to the host computer. This eliminated any electromagnetic interference (EMI) that would have been introduced by the USB bus during data acquisition.
- **Data Collection Size ($\mathcal{N}$):** A total of $\mathcal{N} = 150$ unique data sets were collected per trial. This size was maintained consistently across all experimental steps to ensure statistical validity.
- **Motor Movement Mode:** All data collection was performed using a fixed **forward rotational mode** for the motors. This consistency was maintained because the direction of motor rotation (forward/reverse) might alter the induced magnetic field. Using only one mode therefore mitigates the complexity of bi-directional effects [8].
- **Battery Placement and Charge Level:** The location of the batteries, which are inherently a source of hard-iron distortion, was fixed at the furthest point from the magnetometer to minimize static interference [1]. Furthermore, the battery charge level was consistently maintained to ensure each trial doesn't have a voltage drop larger than 0.5V . Voltage drops across the battery cells limits the power supplied to the motors at a set PWM value, affecting the relationship between PWM and soft-iron distortion.

D. Discussion of Metrics

- **Eccentricity (e):** Soft-iron distortion is quantified by the eccentricity of a two-dimensional ellipse, calculated as $e = \sqrt{1 - (b/a)^2}$, where a and b are the semi-major and semi-minor axis lengths. These values are obtained from an elliptical least-square fit, where manual inspection confirmed no model misspecification occurred. Uncertainty is reported as the standard error across three trials.
- **Hard-Iron Translation (d):** Hard-iron distortion is quantified by the magnitude of the vector required to translate the centre of the data to the origin. The centre of the data is the algebraic centre of the fitted ellipse.
- **Change in Eccentricity (Δe):** The effectiveness of the compensation is quantified by the change in eccentricity between the pre-compensation and post-compensation data sets.
- **Standard Error (SE):** The standard error, $\sigma/\sqrt{n}$, across three independent trials is used to estimate the uncertainty introduced by the stochastic nature of manual rotation and variable sample intervals.

IV. Results

Magnetometer data collected, with PWM values set to 0, 50, 100, and 150, show a near-linear relationship between eccentricity and PWM supplied, shown in Fig. 4. This suggests that the soft-iron distortion induced by the motors increases as the power to the motors increases.

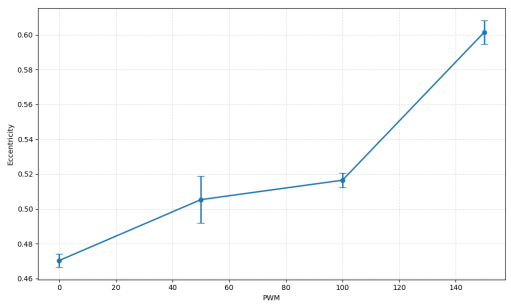

Fig. 4: *Eccentricity plotted against increasing PWM steps, showing the change in soft-iron distortion as the power supplied to the motors is increased.*

There is a clear exception to the linear relationship at 100 PWM, the reason for this is unknown and further data collection would be required to determine if this is an outlier. A linear relationship between PWM and eccentricity would be required to enable compensation for soft-iron distortion to be applied across the entire PWM range without unique data being captured for each PWM. The semi-major and semi-minor axes of the ellipses formed by the dataset obtained at these PWM values is shown in Fig. 5.

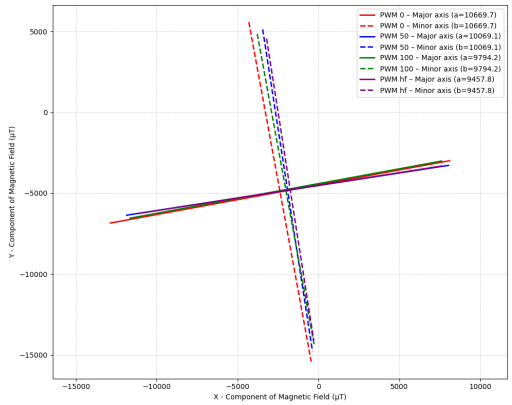

Fig. 5: *Orientations of least-square fitted ellipses for each PWM step. A similar orientation is observed for each PWM.*

These axes show minimal variation in orientation and the centres of the datasets vary minimally with changing PWM. Minimal changes to the centre points of the data suggests that hard-iron distortion is not significantly affected by the power supplied to the motors. The minimal change to axis orientation suggests that, given an estimated eccentricity for each PWM value, the resulting soft-iron compensation matrix can be modelled as a scalar multiple of the baseline (0-PWM) soft-iron matrix. This allows the compensation matrix to be written as

$$S_I^{-1}(PWM) = k(PWM)S_I^{-1}(0),$$

where $k = e(PWM)/e(0)$.

Following the method described in III-B, the hard-iron translation compensation was calculated and applied to each datapoint. Following this, the soft-iron compensation matrix was calculated, and applied to each datapoint. This process, from raw data (red) , $e = 0.472$, to compensated data (blue), $e = 0.061$, is shown in Fig. 6.

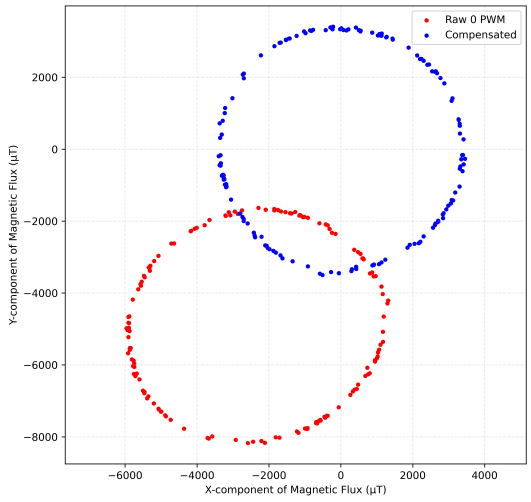

Fig. 6: *Demonstration of the compensation applied (blue) to raw magnetometer readings (red) from 0 PWM.*

The change in eccentricity was recorded as $\Delta e = 0.411$, showing a significant mitigation of the soft-iron distortion inherent to the robot. The same compensation matrix, with a scaling factor equal to the ratio of eccentricity, was then applied to the dataset obtained when the motors were set to 100 PWM, Fig. 7.

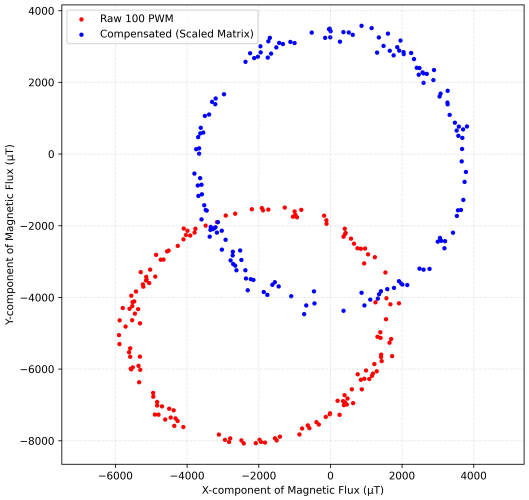

Fig. 7: *Demonstration of the compensation applied (blue) to raw magnetometer readings (red) from 100 PWM, using a scaled version of the matrix acquired from 0 PWM data.*

This graph shows the raw data (red), $e = 0.521$, and the compensated data (blue), $e = 0.225$, demonstrating a clear reduction in soft-iron distortion. The mitigation was not as effective as when a unique compensation matrix was calculated for the dataset, which resulted in an estimated eccentricity of $e = 0.188$. However, as shown in Fig. 8, the scaled compensation matrix applies a similar change to the shape of the data.

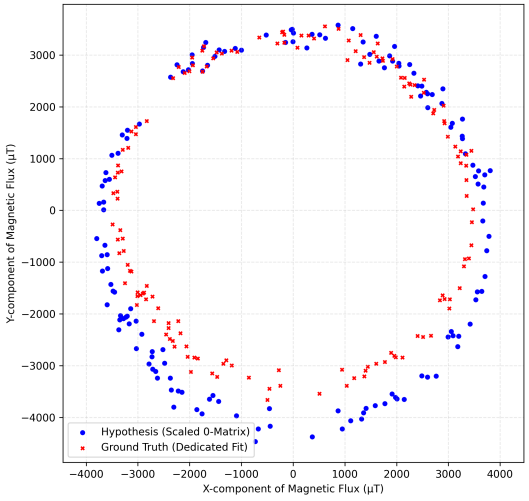

Fig. 8: *Comparison of compensation using a deformation calculated specifically for 100 PWM (red) and a scaled version of the matrix calculated for 0 PWM (blue).*

V. Discussion and Conclusion

Fig. 1 shows clear evidence of both hard-iron and soft-iron distortion, even when the motors are OFF, confirming that the magnetometer readings are inherently influenced by both the surrounding environment and the robot platform itself. Nevertheless, the influence increases when the motors are ON and increases further at higher PWM values,

as shown in Fig. 6. Hard-iron distortion is compensated by re-centering the elliptcal data to (0,0) on a 2D plot.

In this study, the hard-iron distortion compensation proved sufficient for each PWM tested. Therefore, no further attention was given to analysing the relationship between PWM value and the distance of the shift from (0,0), or to quantifying how the amount of hard-iron distortion scales with PWM. In contrast, soft-iron distortion requires a more complex compensation model because the deformed elliptical shape must be transformed back into a circle. This transformation must account not only for the magnitude of deformation but also the orientation of the ellipse. It was discovered that PWM change had minimal impact on the orientation of the ellipse. This allowed a scale factor, proportional to the ratio of ellipticity, to provide significant compensation for the range of soft-iron distortion produced by varying motor power. Identification of a reliable scaling relationship between PWM and eccentricity failed, preventing the implementation of a real-time model for the entire PWM range. However, it was confirmed that with this relationship, one can significantly reduce the soft-iron distortion introduced by the motors over the available PWM range.

These findings support the feasibility of the theory posed in our hypothesis:

> The implementation of the theoretical compensation model to mitigate soft- and hard-iron distortion from magnetometer readings prompts an investigation into the scaling of distortions relative to supplied PWM values. We hypothesise that a compensation model can be created for the 3Pi+ robot that scales proportionally to the PWM supplied to the motors, mitigating both the inherent distortions and those induced by motor activity.

However, finding the PWM-eccentricity relationship, and constructing an exact implementation of this theory remain incomplete.

There were many limitations to the quality of data obtained which likely prevented a linear relationship from being observed between PWM and eccentricity. In an attempt to identify these limitations more explicitly we conducted a small number of additional experiments. These experiments were conducted in various locations, each producing slightly different magnetometer readings, even though the same interference-prevention procedures were applied. As noted in Section III, the core tests were performed indoors in a controlled room away from external interference. For each PWM three trials were operated and it was concluded that having only three trails was not sufficient enough to find a reliable relationship between PWM the distortion behavior. However, performing the experiment outdoors, directly on the ground, might have provided clearer data—particularly for studying the behavior of soft-iron distortion.

Additionally, using an SD card to store larger datasets at each PWM level would have produced a richer dataset. This would have allowed the motors to remain ON for longer periods, enabling investigation of the effects of prolonged motor operation on magnetometer distortion as well.

In conclusion, the models developed in this study reliably compensate for hard-iron distortion at any PWM value and successfully correct soft-iron distortion at specific PWM levels. Furthermore, if a reliable relationship between PWM and eccentricity in the 2D representation can be established, this would enable a predictive mapping model where the expected eccentricity can be inserted into the deformation matrix scaling, and updated live through an onboard algorithm for real-time, PWM dependent, soft-iron compensation during robot operation.

VI. Future Work

Future work could extend this study in several meaningful directions. One approach is to reverse the motor rotation or test alternative motion modes for the left and right wheels to better understand their individual magnetic influence on the magnetometer. Another natural progression is to rotate the robot in a standard three-dimensional compass calibration method, and plot the magnetometer readings in 3D. Then, fit a sphere to the full dataset and investigate how different PWM levels affect spatial deformation. Additionally, observing the effect of introducing the third dimension in the method contained in this paper may add insight to the distortion metrics beyond the 2D projection of the data used here.

Conducting the experiments outdoors may further reduce unwanted environmental interference, providing clearer insight into the true behavior of hard- and soft-iron distortions. Finally, developing a real-time compensation algorithm and testing its practical accuracy, when using the magnetometer as a compass, would provide strong validation of the model. Then, Repeating the entire experiment on different Pololu 3pi+ robots would help determine whether the same distortions occur and whether the proposed model remains effective across platforms.

In summary, this paper provides a strong justification for further investigation into these compensation methods. However, more tests must be carried out to obtain the relationship between PWM and soft-iron distortion before the method can be implemented and tested across different 3Pi+ systems.

References

[1] "Pololu 3pi+ 32u4 user's guide,"

[2] G. Yin and L. Zhang, "Magnetic heading compensation method based on magnetic interferential signal inversion," vol. 275, pp. 1–10.

[3] STMicroelectronics, *LIS3MDL: Digital output magnetic sensor: ultra-low-power, high-performance 3-axis magnetometer*. STMicroelectronics, 2017. Datasheet.

[4] M. J. Caruso, "Applications of magnetic sensors for low cost compass systems," in *IEEE Position Location and Navigation Symposium*, pp. 167–174, IEEE, 2000.

[5] A. Sawicki, Z. Slanina, and A. Linkel, "Compensation of hard- and soft-iron distortions is magnetometer measurement data," p. 104455S.

[6] "Learn more about magnetometer models and HSI calibration · VectorNav."

[7] Pololu Corporation, *Balboa 32U4 Balancing Robot User's Guide: Inertial Sensors*, 2025. Section 3.5: Inertial Sensors. States that the LIS3MDL is affected by magnetic fields from motors and electrical currents.

[8] M. H. Afzal, V. Renaudin, and G. Lachapelle, "Magnetometer calibration using inertial sensors," in *2011 International Conference on Indoor Positioning and Indoor Navigation*, pp. 1–7, IEEE, 2011. Demonstrates that magnetic interference is linearly dependent on the magnitude and polarity of the current drawn by the system.